PET Imaging of Fibroblast Activation Protein in Various Types of Cancer Using ^{68}Ga-FAP-2286: Comparison with ^{18}F-FDG and ^{68}Ga-FAPI-46 in a Single-Center, Prospective Study

Yizhen Pang*[1,2], Liang Zhao*[1,2], Tinghua Meng*[1], Weizhi Xu[1], Qin Lin[2], Hua Wu[1], Jingjing Zhang[3,4], Xiaoyuan Chen[4–6], Long Sun[1], and Haojun Chen[1]

[1]Department of Nuclear Medicine and Minnan PET Center, First Affiliated Hospital of Xiamen University, School of Medicine, Xiamen University, Xiamen, China; [2]Department of Radiation Oncology, First Affiliated Hospital of Xiamen University, Xiamen, China; [3]Department of Diagnostic Radiology, National University of Singapore, Singapore; [4]Clinical Imaging Research Centre, Centre for Translational Medicine, Yong Loo Lin School of Medicine, National University of Singapore, Singapore; [5]Departments of Diagnostic Radiology, Surgery, Chemical and Biomolecular Engineering, and Biomedical Engineering, Yong Loo Lin School of Medicine and Faculty of Engineering, National University of Singapore, Singapore; and [6]Nanomedicine Translational Research Program, NUS Center for Nanomedicine, Yong Loo Lin School of Medicine, National University of Singapore, Singapore

PET imaging that targets fibroblast activation protein (FAP) on the surface of cancer-associated fibroblasts has yielded promising tumor diagnostic results. FAP-2286 contains cyclic peptides as FAP-binding motifs to optimize tumor retention compared with the small-molecule FAP inhibitor (FAPI) series (FAPI-04/46). The aim of this study was to evaluate the diagnostic accuracy of ^{68}Ga-FAP-2286 to detect primary and metastatic lesions in patients with various types of cancer, compared with ^{18}F-FDG and ^{68}Ga-FAP-2286. **Methods:** Sixty-four patients with 15 types of cancer underwent ^{68}Ga-FAP-2286 PET/CT for initial assessment or detection of recurrence. For comparison, 63 patients underwent paired ^{68}Ga-FAP-2286 and ^{18}F-FDG PET/CT and 19 patients underwent paired ^{68}Ga-FAP-2286 and ^{68}Ga-FAPI-46 PET/CT. Lesion uptake was quantified as SUV_{max} and tumor-to-background ratio. The Wilcoxon matched-pairs signed-rank test was used to compare SUV_{max} between PET modalities, and the McNemar test was used to compare lesion detectability. **Results:** Uptake of ^{68}Ga-FAP-2286 was significantly higher than that of ^{18}F-FDG in primary tumors (median SUV_{max}, 11.1 vs. 6.9; $P < 0.001$), lymph node metastases (median SUV_{max}, 10.6 vs. 6.2; $P < 0.001$), and distant metastases, resulting in improved image contrast and lesion detectability. All primary tumors (46/46) were clearly visualized by ^{68}Ga-FAP-2286 PET/CT, whereas 9 of the 46 lesions could not be visualized by ^{18}F-FDG PET/CT. The lesion detection rate of ^{68}Ga-FAP-2286 PET/CT was superior to that of ^{18}F-FDG PET/CT for involved lymph nodes (98% [105/107] vs. 85% [91/107], $P = 0.001$) and bone and visceral metastases (95% [162/171] vs. 67% [114/171], $P < 0.001$). ^{68}Ga-FAP-2286 yielded tumor uptake and lesion detection rates similar to those of ^{68}Ga-FAPI-46 in a subcohort of 19 patients. **Conclusion:** ^{68}Ga-FAP-2286 is a promising FAP-inhibitor derivative for safe cancer diagnosis, staging, and restaging. It may be a better alternative to ^{18}F-FDG for the cancer types that exhibit low-to-moderate uptake of ^{18}F-FDG, which include gastric, pancreatic, and hepatic cancers. In addition, ^{68}Ga-FAP-2286 and ^{68}Ga-FAPI-46 yielded comparable clinical results.

The glucose analog ^{18}F-FDG is extensively used for tumor metabolic imaging. Cancer-associated fibroblasts, one of the most abundant components of the tumor stroma, are alternative targets for the imaging of solid tumors (*1*). Considering the high expression of fibroblast activation protein (FAP) on the cell surfaces of activated cancer-associated fibroblasts and its limited expression in normal tissue, PET imaging of cancer-associated fibroblasts with radiolabeled FAP inhibitors (FAPIs) is an active field in nuclear medicine (*2*).

^{68}Ga- and ^{18}F-radiolabeled FAPI variants (including FAPI-04, FAPI-46, and FAPI-74) have yielded promising results in the diagnosis of various cancers (*3–5*). Furthermore, FAPI has been reported to be superior to ^{18}F-FDG in PET/CT imaging of, for example, hepatic, gastric, and pancreatic cancer, as well as peritoneal carcinomatosis (*6–9*). However, these FAPI molecules are normally retained in tumors for a relatively short time, potentially limiting their use for radionuclide therapy (*10,11*).

FAP-2286 is a low-molecular-weight, FAP-targeted polypeptide linked to the chelator DOTA, which allows for the attachment of radionuclides for imaging and therapeutic use. FAP-2286, developed using a cyclic peptide as a binding motif, is reported to be potent, highly selective for FAP, and stable in human plasma (*12*). In addition, it has a long retention time in tumors, translating to the robust antitumor efficacy of ^{177}Lu-FAP-2286 as demonstrated in a preclinical study (*12*). In this study, FAP-2286 had a half-maximal effective concentration comparable to that of FAPI-46 (4.9 vs. 1.7 nM), as well as better cellular internalization, longer retention, and higher uptake on PET/CT scans at all time points in human embryonic kidney FAP cells. Moreover, ^{177}Lu-FAP-2286 had a significantly higher tumor retention than ^{177}Lu-FAPI-46 at 24 and 72 h after injection, resulting in excellent antitumor efficacy in human

embryonic kidney FAP xenografts. The results of a recent pilot study in which ^{177}Lu-FAP-2286 was used for peptide-targeted radionuclide therapy in patients with diverse advanced adenocarcinomas exhibited acceptable side effects and prolonged retention and activity (13). The preliminary results from the LuMIERE trial (NCT04939610) reported that ^{177}Lu-FAP-2286 demonstrated a manageable safety profile with some promising efficacy in 9 patients with 7 types of cancer (partial response was observed in 1 patient who completed 6 cycles of ^{177}Lu-FAP-2286 in a 3.7-GBq dose cohort) (14). When these results are taken together, FAP-2286 exhibits promising characteristics as a targeting vector, with potent and selective FAP binding that leads to intense tumor accumulation and substantial therapeutic efficacy.

In this study, we aimed to investigate the diagnostic accuracy of the novel imaging agent ^{68}Ga-FAP-2286 for detecting primary and metastatic lesions in patients with various types of cancer, and we compared the results with those of ^{18}F-FDG and ^{68}Ga-FAPI-46.

MATERIALS AND METHODS

Participant Enrollment

This is a preliminary report of an ongoing, single-center, prospective study of the diagnostic accuracy of ^{68}Ga-FAP-2286 for PET/CT imaging of solid tumors. The institutional review board approved the study (approval 2022KY013), and all subjects gave written informed consent. The study was registered at ClinicalTrials.gov (NCT05392205). The inclusion criteria were as follows: adult patients (aged 18 y or older), patients with newly diagnosed or previously treated malignant tumors (to avoid the treatment impact on radiotracer uptake, the interval between the completion of therapy and the PET scan was > 6 mo), and patients who were able to provide informed consent or assent according to the guidelines of the Clinical Research Ethics Committee. Exclusion criteria were as follows: patients with nonmalignant disease; patients who were pregnant; and patients, their parents, or their legal representatives who were unable or unwilling to provide written informed consent.

Radiolabeling

FAP-2286 and FAPI-46 were obtained from Yantai Dongcheng Pharmaceutical Group Co., Ltd., and Jiangsu Huayi Technology Co., Ltd., respectively. Both compounds were used for research purposes. ^{18}F-FDG was manufactured according to the standard method of our laboratory (15,16) using the coincidence ^{18}F-FDG synthesis module (TracerLab FxFN; GE Healthcare). The FAPI-46 ligands were radiolabeled with ^{68}Ga according to a previous protocol (17). Briefly, 925–1,110 MBq of ^{68}GaCl$_3$ eluted from the ^{68}Ge/^{68}Ga generator (ITG) were reacted with 25 μg (28.2 nmol) of FAPI-46 in 1 mL of 0.25 M sodium acetate buffer for 10 min at 100°C and purified before use. FAP-2286 ligands were radiolabeled with ^{68}Ga in a similar protocol (925–1,110 MBq of ^{68}GaCl$_3$ reacted with 25 μg [17.0 nmol] of FAP-2286). The synthesis of the radiopharmaceutical is detailed in the supplemental materials (available at http://jnm.snmjournals.org).

PET/CT Imaging and Evaluation

The dose of intravenously injected ^{68}Ga-FAP-2286 was calculated according to the participants' body weight (1.8–2.2 MBq/kg). At 1 h after intravenous administration, the participants underwent PET/CT via a hybrid scanner (Discovery MI; GE Healthcare). All obtained data were transferred to the Advantage Workstation (version AW 4.7; GE Healthcare) and reconstructed using the Bayesian penalized-likelihood reconstruction algorithm (Q.clear; GE Healthcare). For patients with malignant disease, additional ^{18}F-FDG or ^{68}Ga-FAPI-46 PET/CT was performed for comparative purposes, depending on the patients' willingness. The PET/CT imaging protocols for ^{18}F-FDG and ^{68}Ga-FAPI-46 were the same as those for ^{68}Ga-FAP-2286, except

that 6 h of fasting were required before the ^{18}F-FDG PET/CT scan (the supplemental materials provide details) (18).

All PET images were evaluated by 2 board-certified nuclear medicine physicians, each with at least 10 y of experience in PET/CT imaging; the 2 physicians were not masked to the study. Disagreements in opinion were resolved via discussion and consensus. In addition to visual evaluation, lesions were evaluated semiquantitatively by selection of regions of interest. The SUV$_{max}$ was calculated automatically

TABLE 1
Patients' Characteristics ($n = 64$)

Characteristic	Data
Number of patients	64
Patients with paired ^{68}Ga-FAP-2286 and ^{18}F-FDG PET/CT	63
Days between ^{68}Ga-FAP-2286 and ^{18}F-FDG PET/CT	1–7
Patients with paired ^{68}Ga-FAP-2286 and ^{68}Ga-FAPI-46 PET/CT	19
Days between ^{68}Ga-FAP-2286 and ^{68}Ga-FAPI-46 PET/CT	1–4
Median age (y)	57.5 (range, 32–85)
Sex	
Male	38
Female	26
Types of cancer	
Head and neck	15
Hepatic	12
Gastric	10
Pancreatic	7
Ovarian	5
Esophageal*	4
Breast	3
Non–small cell lung*	2
Renal	2
Glioblastoma	1
Thymic	1
Colorectal	1
Yolk sac tumor	1
Gastrointestinal stromal tumor	1
Clinical reason for PET/CT	
Detection of unknown primary tumor	3
Staging of cancer	39
Evaluation of doubtful lesions	2
Identification of disease recurrence	20
Final diagnosis	
Histopathologic confirmation (via biopsy or surgery)	58
Diagnostic imaging/follow-up	6

*One patient was diagnosed with synchronous double cancer (esophageal and lung adenocarcinoma).
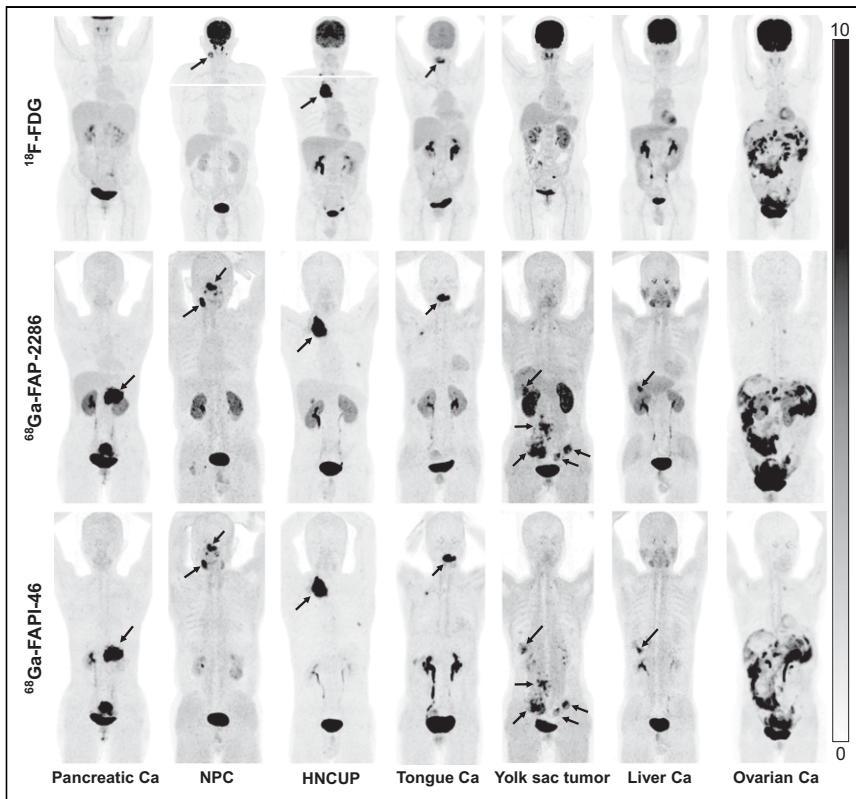
Data are numbers, unless indicated otherwise.

FIGURE 1. Maximum-intensity projections of ^{18}F-FDG, ^{68}Ga-FAP-2286, and ^{68}Ga-FAPI-46 PET/CT imaging in 7 patients with different types of cancer (histologically confirmed). Tumor lesions are indicated with arrows. Ca = carcinoma; HNCUP = head and neck carcinoma of unknown primary; NPC = nasopharyngeal carcinoma.

using the Advantage Workstation. Regions with radiotracer uptake higher than the background activity in primary tumors, lymph nodes, the lungs, the liver, peritoneal surfaces, and other body parts were considered pathologic. Tracer uptake in normal organs (background) was quantified on the basis of SUV_{mean}, which was delineated with a sphere 1 cm in diameter (for the small organs, including thyroid, salivary gland, pancreas) to 2 cm
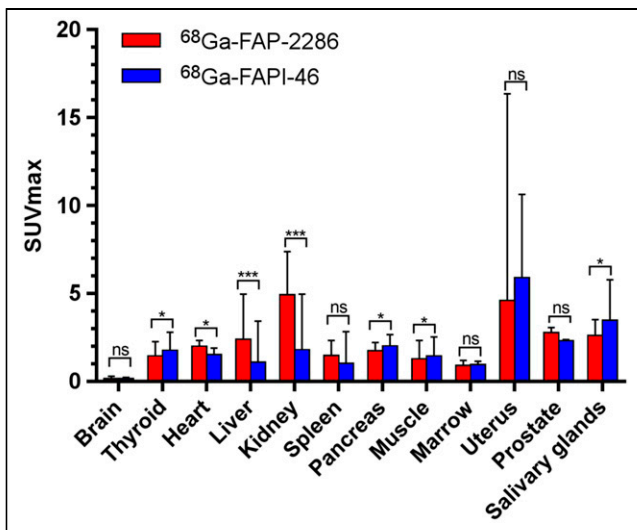
in diameter (for the other organs, including brain, heart, liver, kidney, spleen, muscle, and bone marrow) placed inside the organ parenchyma. The tumor-to-background ratio (TBR) was calculated as the ratio of the tumor SUV_{max} to the background SUV_{mean}. Physiologic uptake of ^{68}Ga-FAP-2286 and ^{68}Ga-FAPI-46 in normal organs was determined by calculating the SUV_{mean} of the background measurements in the heart, liver, spleen, lungs, kidneys, muscles, prostate, and uterus. Histopathologic results obtained via surgery or biopsy served as the gold standard for the final diagnosis. If tissue-based diagnosis was not possible, comprehensive evaluations of multimodal imaging characteristics were used as the reference standard.

Statistical Analysis

Statistics were analyzed using SPSS, version 22.0 (IBM). The Wilcoxon matched-pairs signed-rank test was used to compare SUVs derived from ^{68}Ga-FAP-2286, ^{68}Ga-FAPI-46, and ^{18}F-FDG PET/CT images. The McNemar test was used to compare the lesion detectability of different PET scans. The paired-sample t test was used to evaluate differences in normal-organ uptake between ^{68}Ga-FAP-2286 and ^{68}Ga-FAPI-46 PET/CT. Statistical significance was defined as a P value of less than 0.05.

RESULTS

Patient Characteristics

From March 1, 2022, to May 31, 2022, 64 patients with malignant disease (38 men; median age, 57.5 y; range, 32–85 y) who underwent ^{68}Ga-FAP-2286 PET/CT were enrolled in this prospective study (Table 1). Among the 64 patients, 44 (9 types of cancer) underwent PET/CT for initial assessment (lesion detection and staging) and the other 20 (9 types of cancer) for detection of tumor recurrence and metastases (restaging). The final diagnosis was based on histopathologic results ($n = 58$) and diagnostic radiology (comprehensive considerations of imaging findings, $n = 6$). For comparison, 63 patients underwent paired ^{68}Ga-FAP-2286 and ^{18}F-FDG PET/CT and 19 patients underwent paired ^{68}Ga-FAP-2286 and ^{68}Ga-FAPI-46 PET/CT. Representative images from the 3 types of PET scans are shown in Figure 1.

Adverse Events and Biodistribution

All patients tolerated the ^{68}Ga-FAP-2286 PET/CT scans. There were no signs of any drug-related pharmacologic effects or other adverse physiologic responses. All observed vital signs (including temperature, blood pressure, and heart rate) were normal at the 4-h follow-up. No abnormal symptoms were reported by the patients.

The in vivo distribution pattern of ^{68}Ga-FAP-2286 was evaluated and compared with that of ^{68}Ga-FAPI-46 in 19 patients who underwent both scans. ^{68}Ga-FAP-2286 exhibited an in vivo distribution pattern similar to that of ^{68}Ga-FAPI-46, except for a slightly higher physiologic uptake in the liver and kidneys (Fig. 2). Semiquantitative analysis demonstrated that ^{68}Ga-FAP-2286 uptake in the kidneys (5.3 ± 1.5 vs. 2.3 ± 1.2, $t = 8.959$, $P < 0.001$), liver (2.8 ± 1.0 vs. 1.5 ± 0.9, $t = 8.582$, $P < 0.001$), and heart (1.9 ± 0.4 vs. 1.4 ± 0.3, $t = 6.557$, $P < 0.001$) were higher than that of ^{68}Ga-FAPI-46. In contrast, background uptake of ^{68}Ga-FAP-2286 in the thyroid

FIGURE 2. PET-based biodistribution analysis of ^{68}Ga-FAP-2286 and ^{68}Ga-FAPI-46 in normal organs at 1 h after injection. Results are shown as means and SDs from 19 patients. *$P < 0.05$. ***$P < 0.001$. ns = not statistically significant.

TABLE 2
Comparison of SUV$_{max}$ on ^{68}Ga-FAP-2286 and ^{18}F-FDG PET/CT Images in Primary and Metastatic Tumors

| Tumor type | n | Size (cm) | ^{68}Ga-FAP-2286 | | | ^{18}F-FDG PET/CT | | | P | |
			Positive tumors	SUV$_{max}$	TBR	Positive tumors	SUV$_{max}$	TBR	Median SUV$_{max}$ (FAP-2286 vs. ^{18}F-FDG)	TBR (FAP-2286 vs. ^{18}F-FDG)
Primary										
Total§	46	3.2 (0.9–11.3)	46	11.1 (2.5–28.9)	9.2 (1.1–31.5)	37	6.9 (1.5–19.1)	3.0 (0.9–13.2)	<0.001	<0.001
HNC	7	1.7 (1.5–3.4)	7	16.8 (11.0–20.2)	13.7 (8.1–15.3)	7	11.0 (4.0–15.6)	7.0 (2.9–13.1)	0.043	0.043
Breast cancer*	6	1.5 (0.9–7.0)	6	9.9 (6.0–18.3)	10.1 (3.9–22.3)	4	6.4 (1.5–17.3)	5.0 (1.1–13.2)	0.249	0.075
Esophageal cancer	4	4.1 (2.1–9.0)	4	22.9 (10.0–26.4)	13.6 (6.3–19.4)	4	11.6 (7.9–18.4)	5.8 (4.7–8.6)	0.068	0.068
Lung adenocarcinoma	2	2.9 (1.1–4.7)	2	7.5 (5.7–9.3)	10.0 (9.2–10.9)	2	6.1 (3.3–8.9)	7.1 (4.2–10.0)	NA	NA
Gastric cancer	6	2.0 (1.2–4.5)	6	9.1 (4.1–13.0)	9.2 (4.9–12.7)	3	3.4 (1.7–7.9)	2.0 (0.9–4.1)	0.028	0.028
Hepatic cancer	8	5.2 (0.9–11.3)	8	11.3 (2.5–28.9)	5.2 (1.5–9.4)	5	4.8 (3.1–9.7)	1.5 (1.0–3.5)	0.917	0.028
Pancreatic cancer	7	3.4 (2.4–5.7)	7	13.0 (10.7–22.7)	12.2 (5.7–23.3)	6	6.5 (3.0–8.1)	2.9 (1.1–4.4)	0.018	0.018
Renal cancer	1	4.5 (NA)	1	6.1 (NA)	1.5 (NA)	1	4.1 (NA)	2.0 (NA)	NA	NA
Ovarian cancer	5	4.8 (1.7–6.2)	5	10.8 (6.0–25.6)	11.0 (5.0–31.5)	5	9.6 (5.3–12.2)	6.9 (2.8–9.3)	0.345	0.138
Recurrence/mets										
Recurrent tumor (total†)	9	2.9 (0.7–5.1)	9	5.8 (2.9–16.5)	4.7 (2.2–15.7)	3	3.8 (2.2–7.6)	1.1 (0.8–5.4)	0.015	0.008
LN mets (total)	107	1.2 (0.5–6.6)	105	10.6 (3.0–20.1)	9.0 (2.2–30.0)	91	6.2 (1.3–21.2)	3.7 (1.0–13.0)	<0.001	<0.001
Lung mets	21	0.9 (0.4–1.3)	16	3.4 (0.6–10.2)	4.9 (0.9–14.5)	19	3.5 (0.7–7.1)	5.0 (1.0–10.2)	0.876	0.931
Hepatic mets	30	2.6 (0.9–10.7)	27	6.9 (2.4–12.2)	4.1 (0.9–8.4)	22	6.8 (2.1–10.8)	2.2 (0.9–3.9)	0.484	<0.001
Peritoneal mets	70	NA‡	69	8.6 (2.4–15.4)	6.7 (1.8–27.0)	46	4.6 (1.5–11.4)	2.4 (0.8–8.1)	<0.001	<0.001
Subcutaneous mets	12	0.9 (0.6–2.0)	12	8.1 (5.2–12.4)	9.3 (6.3–20.4)	5	1.4 (0.7–7.4)	1.3 (1.0–11.6)	0.002	0.002
Bone mets	38	1.0 (0.4–3.1)	38	6.6 (3.8–13.3)	10.1 (2.9–26.7)	22	2.7 (0.9–11.4)	2.4 (0.9–19.3)	<0.001	<0.001

*One patient was diagnosed with multifocal breast cancer (4 primary tumors).
†Local recurrent tumors included glioblastoma ($n = 1$), HNC ($n = 4$), hepatic cancer ($n = 3$), and gastric cancer ($n = 1$).
‡Lesion size cannot be calculated because of diffuse type of peritoneal metastases (irregular shape).
§Primary tumors were not located in 2 patients with head and neck cancer of unknown primary etiology; 2 patients were therefore excluded from analysis. Two patients were diagnosed with synchronous double cancer (one with esophageal and lung adenocarcinoma, the other with HNC and renal cancer).
HNC = head and neck cancer; NA = not applicable; mets = metastases; LN = lymph node.
Qualitative data are number; continuous data are median and range.

$(1.6 \pm 0.5$ vs. 1.9 ± 0.5, $t = -3.537$, $P = 0.01$), pancreas $(1.8 \pm 0.3$ vs. 2.1 ± 0.5, $t = -2.559$, $P = 0.038$), muscles $(1.3 \pm 0.5$ vs. 1.5 ± 0.5, $t = -2.515$, $P = 0.04$), and salivary glands $(2.5 \pm 0.6$ vs. 3.6 ± 1.0, $t = -3.356$, $P = 0.012$) were lower than that of ^{68}Ga-FAPI-46 (Fig. 2).

^{68}Ga-FAP-2286 and ^{18}F-FDG Uptake in Cancer Patients

Among the 44 patients who underwent paired ^{68}Ga-FAP-2286 and ^{18}F-FDG PET/CT for initial diagnosis, 1 was diagnosed with a synchronous double cancer (esophageal cancer and lung adenocarcinoma) and 1 was diagnosed with multifocal breast cancer (4 primary tumors in the same breast). In addition, the primary tumors could not be located in 2 patients with head and neck cancers of unknown primary. Thus, in total, 46 primary tumor lesions (all confirmed by histopathology) were evaluated in this study (Table 2). All primary tumors were clearly visualized with intense radiotracer uptake on ^{68}Ga-FAP-2286 PET/CT, whereas 9 of the 46 lesions could not be visualized via ^{18}F-FDG PET/CT. Primary tumor lesions exhibiting no pathologic uptake on ^{18}F-FDG PET/CT images were gastric cancer ($n = 3$), hepatic cancer ($n = 3$), breast cancer ($n = 2$), and pancreatic cancer ($n = 1$) (Supplemental Fig. 1). The SUV$_{max}$ of all primary tumor lesions derived from ^{68}Ga-FAP-2286 PET/CT was significantly higher than that derived from ^{18}F-FDG PET/CT (11.1 vs. 6.9, $P < 0.001$). Moreover, lesions exhibited a 3-fold higher TBR on ^{68}Ga-FAP-2286 PET/CT images than they did on ^{18}F-FDG PET/CT images (9.2 vs. 3.0, $P < 0.001$), thus improving the image contrast for tumor detection and delineation. Representative images are shown in Supplemental Figure 2.

We investigated tumor uptake over time by performing ^{68}Ga-FAP-2286 PET at multiple time points (0.5, 1, and 3 h after injection) in patients 33 and 54. The SUV$_{max}$ in patient 33 (nasopharyngeal carcinoma with lymph node and bone metastases) increased from 0.5 to 3 h in the primary tumor (by 72.1%, from 8.6 to 14.8), involved lymph nodes (by 5.2%–69.1%), and 1 bone metastasis (by 64.4%) (Fig. 3). Similar results were observed in patient 54 (metastatic colon cancer); the hepatic metastases demonstrated stable ^{68}Ga-FAP-2286 uptake but an increased TBR from 1 to 3 h (Supplemental Fig. 3).

Among the 19 patients who underwent paired ^{68}Ga-FAP-2286 and ^{18}F-FDG PET/CT for cancer restaging, ^{68}Ga-FAP-2286 demonstrated significantly higher lesion detection rates than ^{18}F-FDG PET/CT (100% [9/9] vs. 33% [3/9], $P = 0.031$) in 9 locally recurrent tumors (all confirmed by histopathology) (Supplemental Fig. 2B). Among the 63 patients who underwent paired ^{68}Ga-FAP-2286 and ^{18}F-FDG PET/CT for initial staging or restaging, 107 lymph node metastases and 171 bone and visceral metastases were evaluated. Among these, 66 metastatic lesions (12 lymph nodes and 54 bone and visceral metastases) were confirmed by histopathology, and 212 lesions (95 lymph nodes and 117 bone and visceral metastases) were confirmed by diagnostic radiology. ^{68}Ga-FAP-2286 yielded significantly higher radiotracer uptake (SUV$_{max}$, 10.6 vs. 6.2; $P < 0.001$) and TBR (9.0 vs. 3.7, $P < 0.001$) than did ^{18}F-FDG in the metastatic lymph nodes. Therefore, ^{68}Ga-FAP-2286 PET/CT had a significantly higher detection rate (98% [105/107] vs. 85% [91/107], $P = 0.001$) than ^{18}F-FDG PET/CT in the diagnosis of lymph node metastases. Interestingly, the ^{18}F-FDG uptake was positive and the ^{68}Ga-FAP-2286 uptake was negative in the enlarged mediastinal lymph nodes in 1 patient with gastric cancer; these lymph nodes were confirmed to be inflammatory on endobronchial ultrasound-guided transbronchial needle aspiration (Supplemental Fig. 2C). Regarding PET/CT imaging of bone and visceral metastases, ^{68}Ga-FAP-2286 yielded a greater number of positive lesions (95% [162/171] vs. 67% [114/171], $P < 0.001$) and a higher radiotracer uptake and TBR than ^{18}F-FDG in most lesions (hepatic, peritoneal, subcutaneous, and bone metastases). Interestingly, no significant difference in hepatic metastasis SUV$_{max}$ was observed between ^{68}Ga-FAP-2286 and ^{18}F-FDG, even though the TBR yielded by ^{68}Ga-FAP-2286 (4.1) was twice that yielded by ^{18}F-FDG in those lesions (2.2, $P < 0.001$).

With the new lymph node and visceral metastases detected by ^{68}Ga-FAP-2286 PET/CT, TNM staging was upgraded in 3 patients (3/44, 7%), including 1 with gastric cancer (from IIA to IIB), 1 with esophageal cancer (from IIIA to IIIB), and 1 with nasopharyngeal cancer (from IVA to IVB). Compared with ^{18}F-FDG, ^{68}Ga-FAP-2286 PET/CT detected a greater number of metastatic lesions or a larger disease extent in

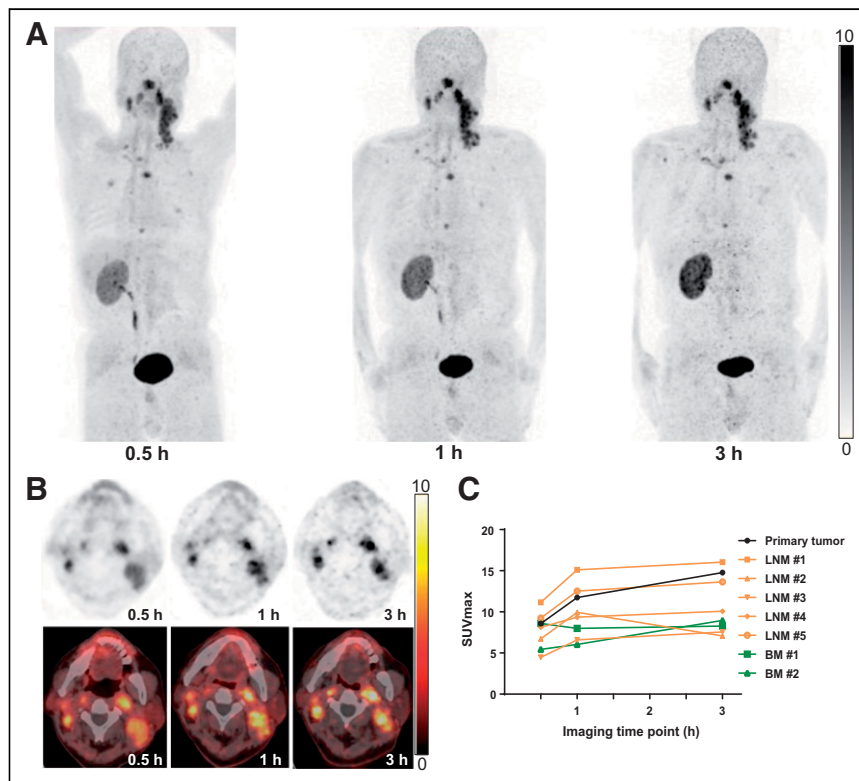**FIGURE 3.** A 66-y-old man with nasopharyngeal carcinoma who underwent ^{68}Ga-FAP-2286 PET/CT at different time points after injection. Rapid and stable radiotracer uptake was observed in both primary and metastatic lesions. Semiquantitative analysis demonstrated SUV$_{max}$ increase at 0.5–3 h in primary tumor (by 72.1% [from 8.6 to 14.8]), involved lymph nodes (by 5.2%–69.1%), and 1 bone metastasis (by 64.4%). BM = bone metastasis; LNM = lymph node metastasis.

12 patients (12/44, 27%), including 4 with pancreatic cancer, 2 with hepatic cancer, 2 with nasopharyngeal cancer, 1 with esophageal cancer, 2 with ovarian cancer, and 1 with gastric cancer. Among the other 19 patients in whom recurrence was detected, ^{68}Ga-FAP-2286 PET/CT detected ^{18}F-FDG–negative locally recurrent tumors in 6 patients (6/19, 32%) and ^{18}F-FDG–negative metastatic lesions in 7 patients (7/19, 37%). The patients with new lesions or a larger disease extent detected by ^{68}Ga-FAP-2286 PET/CT are presented in Supplemental Table 1.

^{68}Ga-FAP-2286 and ^{68}Ga-FAPI-46 Uptake in Patients with Cancer

Among the 19 patients who underwent paired ^{68}Ga-FAP-2286 and ^{68}Ga-FAPI-46 PET/CT, 11 did so for initial staging and 8 for restaging. The ^{68}Ga-FAP-2286–derived SUV_{max} was comparable to that derived from ^{68}Ga-FAPI-46 in 13 primary tumor lesions (13.6 vs. 13.3, $P = 0.53$; Table 3), 4 recurrent tumors (11.2 vs. 9.6, $P = 0.47$), and 33 metastatic lymph nodes (8.3 vs. 8.2, $P = 0.28$). Too few patients with each cancer type underwent paired analyses with these modalities to allow for comparisons of radiotracer uptake per tumor type. Regarding visceral and bone metastases, the quantitative tumor uptake of ^{68}Ga-FAP-2286 was not inferior to that of ^{68}Ga-FAPI-46 in the lung (4.0 vs. 3.9), liver (4.6 vs. 4.4), peritoneum (9.8 vs. 11.4), or bone (6.9 vs. 5.8) (all $P > 0.05$; Table 3). Interestingly, in 1 patient with metastatic cholangiocarcinoma, the median SUV_{max} of ^{68}Ga-FAP-2286 was significantly higher than that of ^{68}Ga-FAPI-46 (8.1 vs. 6.0, $P = 0.022$) in the widespread subcutaneous metastases, and ^{68}Ga-FAP-2286 PET/CT detected a greater number of subcutaneous metastases than ^{68}Ga-FAPI-46 (25 vs. 16). Representative images are shown in Figures 4–6.

DISCUSSION

In this study, we conducted clinical investigations using ^{68}Ga-FAP-2286 for PET/CT imaging in patients with different types of cancer. We aimed to investigate whether ^{68}Ga-FAP-2286 could be used for cancer imaging, and we compared it with ^{18}F-FDG and ^{68}Ga-FAPI-46.

The encouraging results from a preclinical study and a first-in-humans study (12,13) warranted further clinical evaluation of ^{68}Ga-FAP-2286. Therefore, we are in the process of investigating the diagnostic accuracy of ^{68}Ga-FAP-2286 for the identification of FAP-positive solid tumors via PET/CT. First, we evaluated the in vivo distribution pattern of ^{68}Ga-FAP-2286 and compared it with that of ^{68}Ga-FAPI-46. The physiologic uptake of ^{68}Ga-FAP-2286 was lower than that of ^{68}Ga-FAPI-46 in the muscles, salivary glands, thyroid, and pancreas. However, ^{68}Ga-FAP-2286 uptake in the kidneys, liver, and heart was higher than that of ^{68}Ga-FAPI-46, thus suggesting that the cyclopeptide structure of FAP-2286 may lead to altered in vivo pharmacokinetics. Cyclic peptides may have improved biologic properties compared with the small-molecule

TABLE 3
Comparison of SUV$_{max}$ on FAP-2286 and FAPI-46 PET/CT Images in Primary and Metastatic Lesions

Parameter	n	Tumor size (cm)	Tracer	Positive lesions	SUV$_{max}$	P
Primary tumors (total)*	13	3.6 (1.0–6.2)	FAP-2286		13.6 (2.5–25.8)	0.53
			FAPI-46		13.3 (2.4–21.8)	
Recurrence/mets						
Recurrent tumor (total)†	4	3.1 (2.6–5.1)	FAP-2286	4	11.2 (2.7–14.4)	0.465
			FAPI-46	4	9.6 (2.9–13.6)	
Lymph node mets (total)	33	1.2 (0.6–4.6)	FAP-2286	33	8.3 (3.4–15.6)	0.28
			FAPI-46	33	8.2 (4.0–15.4)	
Lung mets	2	0.9 (0.8–1.0)	FAP-2286	2	4.0 (3.8–4.2)	NA
			FAPI-46	2	3.9 (3.6–4.2)	
Hepatic mets	6	2.0 (0.9–11.8)	FAP-2286	6	4.6 (2.7–7.2)	0.345
			FAPI-46	6	4.4 (2.9–8.5)	
Subcutaneous mets	10	0.8 (0.6–2.0)	FAP-2286	10	8.1 (7.4–10.3)	0.022
			FAPI-46	10	6.0 (3.6–8.6)	
Peritoneal mets	22	NA‡	FAP-2286	22	9.8 (6–15.4)	0.18
			FAPI-46	22	11.4 (7.4–19.2)	
Bone mets	10	1.3 (0.7–2.5)	FAP-2286	10	6.9 (3.9–12.2)	0.074
			FAPI-46	10	5.8 (2.9–11.4)	

*Primary tumors included head and neck cancer ($n = 2$), esophageal cancer ($n = 1$), lung adenocarcinoma ($n = 1$), hepatic cancer ($n = 2$), gastric cancer ($n = 1$), pancreatic cancer ($n = 4$), renal cancer ($n = 1$), and ovarian cancer ($n = 1$).
†Including glioblastoma, tongue cancer, hepatic cancer, and gastric cancer.
‡Because peritoneal metastases were statistically analyzed according to peritoneal cancer index score, size of lesions could not be obtained.
Mets = metastases; NA = not applicable.
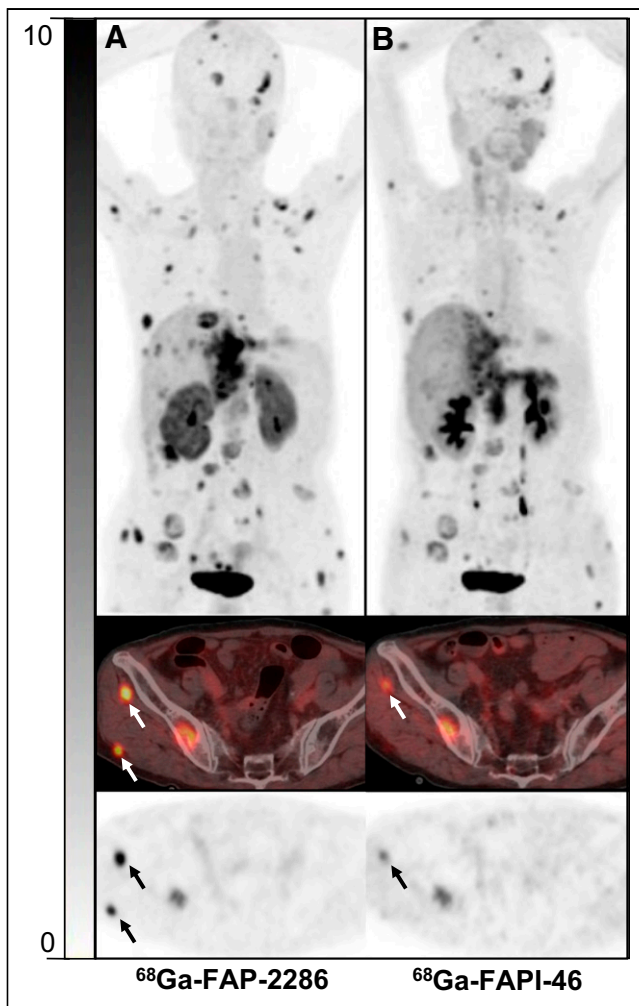Qualitative data are number; continuous data are median and range.

FIGURE 4. A 65-y-old woman with metastatic intrahepatic cholangiocarcinoma who underwent imaging for cancer restaging. ^{68}Ga-FAP-2286 (A) revealed greater number of metastases and higher uptake than ^{68}Ga-FAPI-46 (B) in widespread subcutaneous metastases (arrows).

FIGURE 5. A 72-y-old man with newly diagnosed nasopharyngeal carcinoma who underwent PET/CT for tumor staging. ^{68}Ga-FAP-2286 PET/CT (A) showed higher radiotracer uptake in primary tumor (SUV_{max}, 17.4 vs. 12.2; arrows) than ^{68}Ga-FAPI-46 (B).

FAPI series (*19*), including stronger receptor selectivity and binding affinity, because of increased plasma stability and conformational rigidity. Indeed, ^{177}Lu-FAP-2286 had a long effective half-life in the first-in-humans study (35 ± 9 h in the entire body and 44 ± 25 h in bone metastases) (*13*). Moreover, tumor uptake in our study increased in one patient and remained stable in the other from 0.5 to 3 h after injection. In preclinical studies, FAP-2286 demonstrated longer tumor retention than FAPI-46 at later time points (*12*), and greater antitumor efficacy was observed in tumor xenografts with ^{177}Lu-FAP-2286 than with ^{177}Lu-FAPI-46. When these results are taken together, an increased FAP-binding affinity, improved tumor accumulation, and longer tumor retention are seen to be the main potential advantages of FAP-2286 compared with other FAPI variants. In our study, the results from PET imaging demonstrated that tumor uptake of ^{68}Ga-FAPI-46 and ^{68}Ga-FAP-2286 was comparable at earlier time points, thus indicating that both compounds can be used for imaging of FAP-positive tumors. Further studies with a larger patient population are needed to test the role of ^{68}Ga-FAP-2286 among the existing FAPI derivatives.
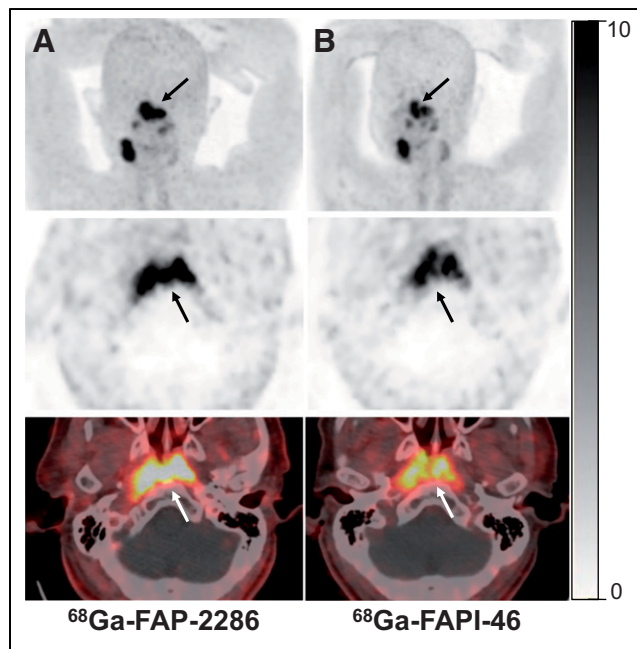
Another aim of the present study was to compare tumor uptake and lesion detectability between ^{68}Ga-FAP-2286 and ^{18}F-FDG PET/CT. With respect to primary tumor lesions, the quantitative tumor uptake and TBR were significantly higher with ^{68}Ga-FAP-2286 than with ^{18}F-FDG. This finding corresponds to the results showing that all primary tumors (46/46) were identified with ^{68}Ga-FAP-2286 whereas 9 were missed with ^{18}F-FDG (Supplemental Fig. 1). Consistent with previous FAPI-based imaging studies (*7–9*), ^{68}Ga-FAP-2286 PET/CT was superior to ^{18}F-FDG PET/CT in gastrointestinal malignancies, including gastric, pancreatic, and hepatic cancer. This result suggests that ^{68}Ga-FAP-2286 PET/CT is promising in the diagnosis of these cancer types for which ^{18}F-FDG PET/CT is inadequate. Regarding the detection of lymph node and visceral metastases, ^{68}Ga-FAP-2286 yielded a higher radiotracer uptake and TBR than ^{18}F-FDG and an improved lesion detectability, particularly of hepatic, bone, and peritoneal metastases. Interestingly, we noted that 1 patient (Supplemental Fig. 2C) with reactive lymph nodes did not exhibit increased ^{68}Ga-FAP-2286 uptake, whereas false-positive ^{18}F-FDG uptake was observed in these nodules. Similar findings have been reported in previous studies (*20*). Thus, we speculate that ^{68}Ga-FAP-2286 may be more suitable than ^{18}F-FDG for differentiating reactive lymph nodes from tumor metastatic lymph nodes. However, tumor and inflammation differentiation by ^{68}Ga-FAP-2286 PET/CT was not the main aim of this study, although this question should be investigated in future clinical trials.

Overall, the results from this study suggest that ^{68}Ga-FAP-2286 is a promising FAPI molecule for cancer diagnosis, staging, and restaging. Therefore, ^{68}Ga-FAP-2286 PET/CT may contribute to the diagnosis of solid tumors, especially in malignant tumors with low-to-moderate uptake on ^{18}F-FDG PET/CT. The specific cancer types that showed ^{68}Ga-FAP-2286 to be superior to ^{18}F-FDG
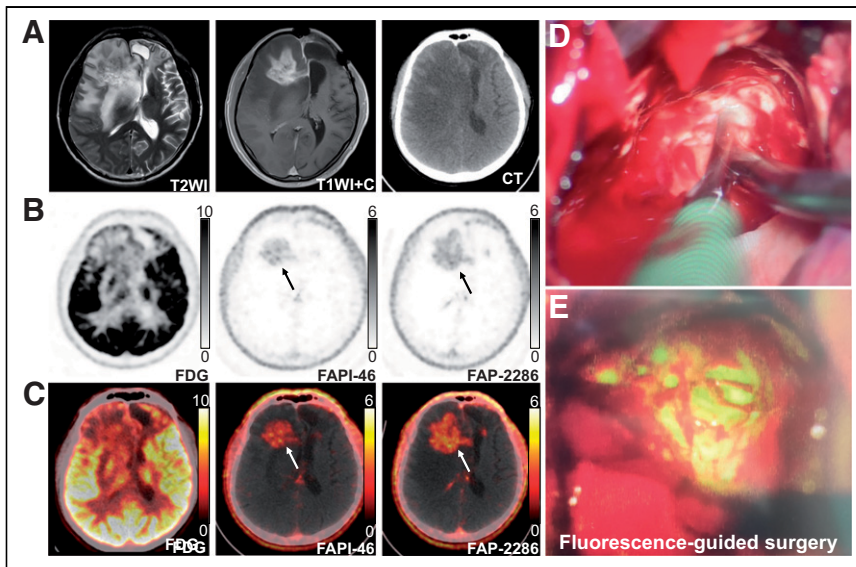
FIGURE 6. A 44-y-old man with glioblastoma who underwent surgical resection 1 y before images were obtained. (A) MRI revealed suggestive recurrent lesions in right frontal lobe adjacent to surgical margin (arrow). (B [axial PET image] and C [fused PET/CT image]) ^{68}Ga-FAP-2286 PET/CT yielded higher radiotracer uptake (SUV$_{max}$, 4.2 vs. 2.7; arrows) and TBR (70.0 vs. 45.0) than ^{68}Ga-FAPI-46 in these lesions. (D [intraoperative view] and E [fluorescence-guided surgery]) Patient subsequently underwent surgical resection, and postoperative pathology confirmed diagnosis of recurrent glioblastoma. T1WI+C = T1-weighted imaging with contrast enhancement; T2WI = T2-weighted imaging.

include gastric, pancreatic, and hepatic cancers; the respective findings were in line with those described in previous publications (7). Specifically, pancreatic and hepatic cancers (especially intrahepatic cholangiocarcinoma) are characterized by intense stromal desmoplastic reactions surrounding cancer cells, and cancer-associated fibroblast are the main effector cells in the desmoplastic reaction (21,22). Furthermore, because of the low background uptake in hepatic parenchyma, FAP imaging was able to detect hepatic tumors with favorable tumor-to-background contrast. Gastric cancer evokes the production and deposition of activated fibroblasts in the submucosa wall (23), resulting in increased ^{68}Ga-FAPI uptake in gastric tumor lesions. Unlike ^{18}F-FDG, very low ^{68}Ga-FAPI uptake was observed in the gastric wall and gastrointestinal tract, which further improved the detectability of gastric cancer. Taken together, high FAP expression and low background activity in abdominal organs are the main reasons and explain why ^{68}Ga-FAP-2286 PET/CT is superior to ^{18}F-FDG in terms of tumor detectability in these tumor entities. Improved tumor detectability may lead to changes in clinical staging and optimization of therapeutic strategies. Moreover, the favorable TBR may improve delineation of gross tumors in radiotherapy and evaluation of the effectiveness of therapy (24,25).

Our study was associated with several limitations. First, few patients underwent paired ^{68}Ga-FAP-2286 and ^{18}F-FDG PET/CT, rendering subgroup analysis of radiotracer uptake per tumor type impracticable. Second, as the subcohort of patients who underwent paired ^{68}Ga-FAP-2286 and ^{68}Ga-FAPI-46 PET/CT was also small ($n = 19$), only a descriptive comparison was possible. Furthermore, as only 2 patients underwent ^{68}Ga-FAP-2286 PET/CT at multiple time points, we could not fully investigate radiotracer retention in tumors. Prospective studies with a larger patient population are warranted to better explore the role of ^{68}Ga-FAP-2286 in cancer diagnosis and the potential superiority of FAP-2286 with respect to other FAPI derivatives.

> **KEY POINTS**
>
> **QUESTION:** Is ^{68}Ga-FAP-2286 an efficacious alternative for the imaging of FAP-positive tumors?
>
> **PERTINENT FINDINGS:** In this preliminary report of a single-center, prospective study of the diagnostic accuracy of ^{68}Ga-FAP-2286 PET/CT of solid tumors, all 46 primary tumors in 9 types of cancer were identified with ^{68}Ga-FAP-2286, whereas 9 were missed with ^{18}F-FDG. ^{68}Ga-FAP-2286 yielded a higher radiotracer uptake and TBR than ^{18}F-FDG. ^{68}Ga-FAP-2286 and ^{68}Ga-FAPI-46 yielded comparable clinical results.
>
> **IMPLICATIONS FOR PATIENT CARE:** ^{68}Ga-FAP-2286 is a promising FAP-inhibitor derivative for safe cancer diagnosis, staging, and restaging.

REFERENCES

1. Backhaus P, Gierse F, Burg MC, et al. Translational imaging of the fibroblast activation protein (FAP) using the new ligand [^{68}Ga]Ga-OncoFAP-DOTAGA. *Eur J Nucl Med Mol Imaging.* 2022;49:1822–1832.
2. Kratochwil C, Flechsig P, Lindner T, et al. ^{68}Ga-FAPI PET/CT: tracer uptake in 28 different kinds of cancer. *J Nucl Med.* 2019;60:801–805.
3. Li M, Younis MH, Zhang Y, Cai W, Lan X. Clinical summary of fibroblast activation protein inhibitor-based radiopharmaceuticals: cancer and beyond. *Eur J Nucl Med Mol Imaging.* 2022;49:2844–2868.
4. Pang Y, Zhao L, Luo Z, et al. Comparison of ^{68}Ga-FAPI and ^{18}F-FDG uptake in gastric, duodenal, and colorectal cancers. *Radiology.* 2021;298:393–402.
5. Zhao L, Chen J, Pang Y, et al. Fibroblast activation protein-based theranostics in cancer research: a state-of-the-art review. *Theranostics.* 2022;12:1557–1569.
6. Shi X, Xing H, Yang X, et al. Comparison of PET imaging of activated fibroblasts and ^{18}F-FDG for diagnosis of primary hepatic tumours: a prospective pilot study. *Eur J Nucl Med Mol Imaging.* 2021;48:1593–1603.
7. Chen H, Pang Y, Wu J, et al. Comparison of [^{68}Ga]Ga-DOTA-FAPI-04 and [^{18}F]FDG PET/CT for the diagnosis of primary and metastatic lesions in patients with various types of cancer. *Eur J Nucl Med Mol Imaging.* 2020;47:1820–1832.

8. Pang Y, Zhao L, Shang Q, et al. Positron emission tomography and computed tomography with [68Ga]Ga-fibroblast activation protein inhibitors improves tumor detection and staging in patients with pancreatic cancer. *Eur J Nucl Med Mol Imaging.* 2022;49:1322–1337.

9. Qin C, Shao F, Gai Y, et al. 68Ga-DOTA-FAPI-04 PET/MR in the evaluation of gastric carcinomas: comparison with 18F-FDG PET/CT. *J Nucl Med.* 2022;63: 81–88.

10. Loktev A, Lindner T, Burger EM, et al. Development of fibroblast activation protein-targeted radiotracers with improved tumor retention. *J Nucl Med.* 2019;60: 1421–1429.

11. Fu K, Pang Y, Zhao L, et al. FAP-targeted radionuclide therapy with [177Lu]Lu-FAPI-46 in metastatic nasopharyngeal carcinoma. *Eur J Nucl Med Mol Imaging.* 2022;49:1767–1769.

12. Zboralski D, Hoehne A, Bredenbeck A, et al. Preclinical evaluation of FAP-2286 for fibroblast activation protein targeted radionuclide imaging and therapy. *Eur J Nucl Med Mol Imaging.* 2022;49:3651–3667.

13. Baum RP, Schuchardt C, Singh A, et al. Feasibility, biodistribution, and preliminary dosimetry in peptide-targeted radionuclide therapy of diverse adenocarcinomas using 166Lu-FAP-2286: first-in-humans results. *J Nucl Med.* 2022;63:415–423.

14. McConathy J, Dhawan M, Goenka A, et al. 177Lu-FAP-2286 in patients with advanced or metastatic solid tumors: initial data from a phase 1/2 study investigating safety, pharmacokinetics, dosimetry, and preliminary antitumor activity (LuMI-ERE) [abstract]. *J Nucl Med.* 2022;63(suppl 2):2271.

15. Zhao L, Zhuang Y, Fu K, et al. Usefulness of [18F]fluorodeoxyglucose PET/CT for evaluating the PD-L1 status in nasopharyngeal carcinoma. *Eur J Nucl Med Mol Imaging.* 2020;47:1065–1074.

16. Yu S. Review of F-FDG synthesis and quality control. *Biomed Imaging Interv J.* 2006;2:e57.

17. Meyer C, Dahlbom M, Lindner T, et al. Radiation dosimetry and biodistribution of 68Ga-FAPI-46 PET imaging in cancer patients. *J Nucl Med.* 2020;61:1171–1177.

18. Boellaard R, Delgado-Bolton R, Oyen WJ, et al. FDG PET/CT: EANM procedure guidelines for tumour imaging: version 2.0. *Eur J Nucl Med Mol Imaging.* 2015; 42:328–354.

19. Parker MFL, Blecha J, Rosenberg O, Ohliger M, Flavell RR, Wilson DM. Cyclic 68Ga-labeled peptides for specific detection of human angiotensin-converting enzyme 2. *J Nucl Med.* 2021;62:1631–1637.

20. Zhou X, Wang S, Xu X, et al. Higher accuracy of [68Ga]Ga-DOTA-FAPI-04 PET/CT comparing with 2-[18F]FDG PET/CT in clinical staging of NSCLC. *Eur J Nucl Med Mol Imaging.* 2022;49:2983–2993.

21. Guo W, Pang Y, Yao L, et al. Imaging fibroblast activation protein in liver cancer: a single-center post hoc retrospective analysis to compare [68Ga]Ga-FAPI-04 PET/CT versus MRI and [18F]-FDG PET/CT. *Eur J Nucl Med Mol Imaging.* 2021; 48:1604–1617.

22. Nielsen MF, Mortensen MB, Detlefsen S. Key players in pancreatic cancer-stroma interaction: cancer-associated fibroblasts, endothelial and inflammatory cells. *World J Gastroenterol.* 2016;22:2678–2700.

23. Zhang J, Li S, Zhao Y, et al. Cancer-associated fibroblasts promote the migration and invasion of gastric cancer cells via activating IL-17a/JAK2/STAT3 signaling. *Ann Transl Med.* 2020;8:877.

24. Windisch P, Zwahlen DR, Koerber SA, et al. Clinical results of fibroblast activation protein (FAP) specific PET and implications for radiotherapy planning: systematic review. *Cancers (Basel).* 2020;12:2629.

25. Zhao L, Pang Y, Zheng H, et al. Clinical utility of [68Ga]Ga-labeled fibroblast activation protein inhibitor (FAPI) positron emission tomography/computed tomography for primary staging and recurrence detection in nasopharyngeal carcinoma. *Eur J Nucl Med Mol Imaging.* 2021;48:3606–3617.